Year-to-Year Changes of Vertical Temperature Distribution in the California Current Region: 1954 to 1986

Jerrold G. Norton and Douglas R. McLain

Studies by Enfield and Allen (1980), McLain *et al* (1985), and others have shown that anomalously warm years in the northern coastal California Current correspond to El Niño conditions in the equatorial Pacific Ocean. Ocean model studies suggest a mechanical link between the northern coastal California Current and the equatorial ocean through long waves that propagate cyclonically along the ocean boundary (McCreary 1976; Clarke 1983; Shriver *et al* 1991). However, distinct observational evidence of such an oceanic connection is not extensive. Much of the supposed El Niño variation in temperature and sea level data from the coastal California Current region (Figure 1) can be associated with the effects of anomalously intense north Pacific atmospheric cyclogenesis, which is frequently augmented during El Niño years (Wallace and Gutzler 1981; Simpson 1983; Emery and Hamilton 1984). This study uses time series of ocean temperature data to distinguish between locally forced effects, initiated by north Pacific atmospheric changes, and remotely forced effects, initiated by equatorial Pacific atmospheric changes related to El Niño events.

Data Series

Seven time series of monthly mean values from 1953 to 1986 were developed for correlation studies. These were five series of average regional ocean temperature at 0, 50, 100, 200 and 300 meter depths and two series of sea level atmospheric pressure (SLP): one from Darwin, Australia (12.4°S x 130.9°E), and the other from 45°N x 165°W in the northeastern Pacific (Figure 2).

For the ocean temperature series, 1.9×10^4 ocean temperature profiles were extracted from the U.S. Navy Fleet Numerical Oceanographic Center Master Oceanographic Observation Data Set (version 4) for the study region and sorted into six subareas (Figure 1). Monthly mean anomaly values were computed from the profile information and divided by the standard deviation of the monthly means at each depth and for each subarea. This allows intercomparison of depths and equal weighting between subareas. Unit magnitude of standardized anomaly (1 sdu) is about 1.0°C above 50 meters, 0.6°C at 100 meters, and 0.5°C below 150 meters.

In: K.T. Redmond and V.L. Tharp, Editors. 1993. Proceedings of the Ninth Annual Pacific Climate (PACLIM) Workshop, April 21-24, 1992. California Department of Water Resources, Interagency Ecological Studies Program, Technical Report 34.

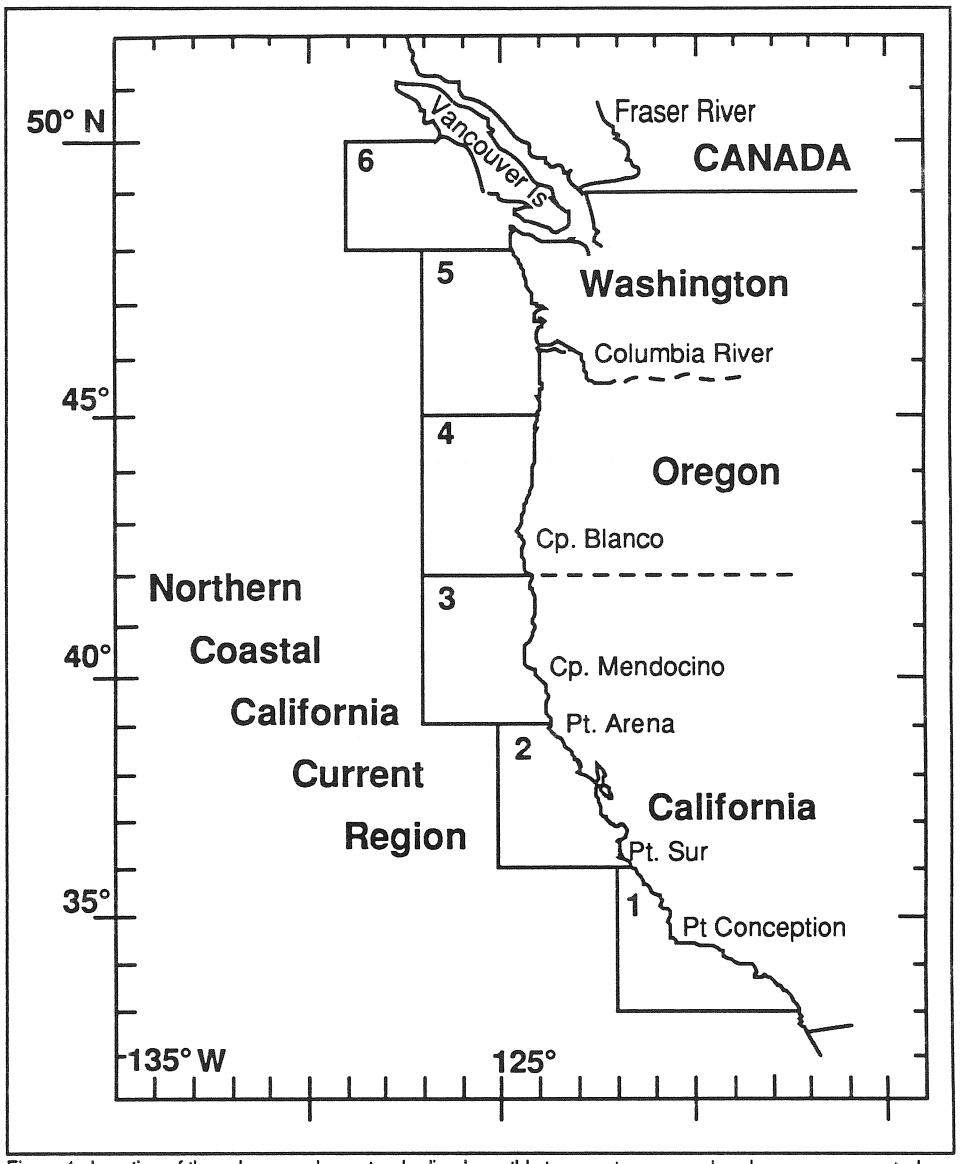

Figure 1. Location of the subareas where standardized monthly temperature anomaly values were computed.

The standardized anomalies for the six subareas were averaged to give a single monthly anomaly value, representative of the entire northern coastal California Current region. Monthly anomalies for the entire region were then averaged to give a single standardized anomaly value ($A_{z,yr}$) for the 6-month (September through February) fall and winter seasons. This value was computed for each depth (z) and year (yr). The above data-averaging processes focuses analysis on environmental events of greater than a 6-month period. Equal weighting of the six subareas brings emphasis to large-scale processes that tend to have areawide coherence. The year designation for the fall/winter period (yr) is that of the fall.

The SLP at Darwin, Australia, is a frequently used indicator of Indonesian Low pressure system development and strength of the equatorial trade winds (Trenberth 1984). The rationale for using this indicator of equatorial Pacific forcing is that an increase in SLP at Darwin is one of the early steps in a sequence of processes that may lead to anomalous warming or

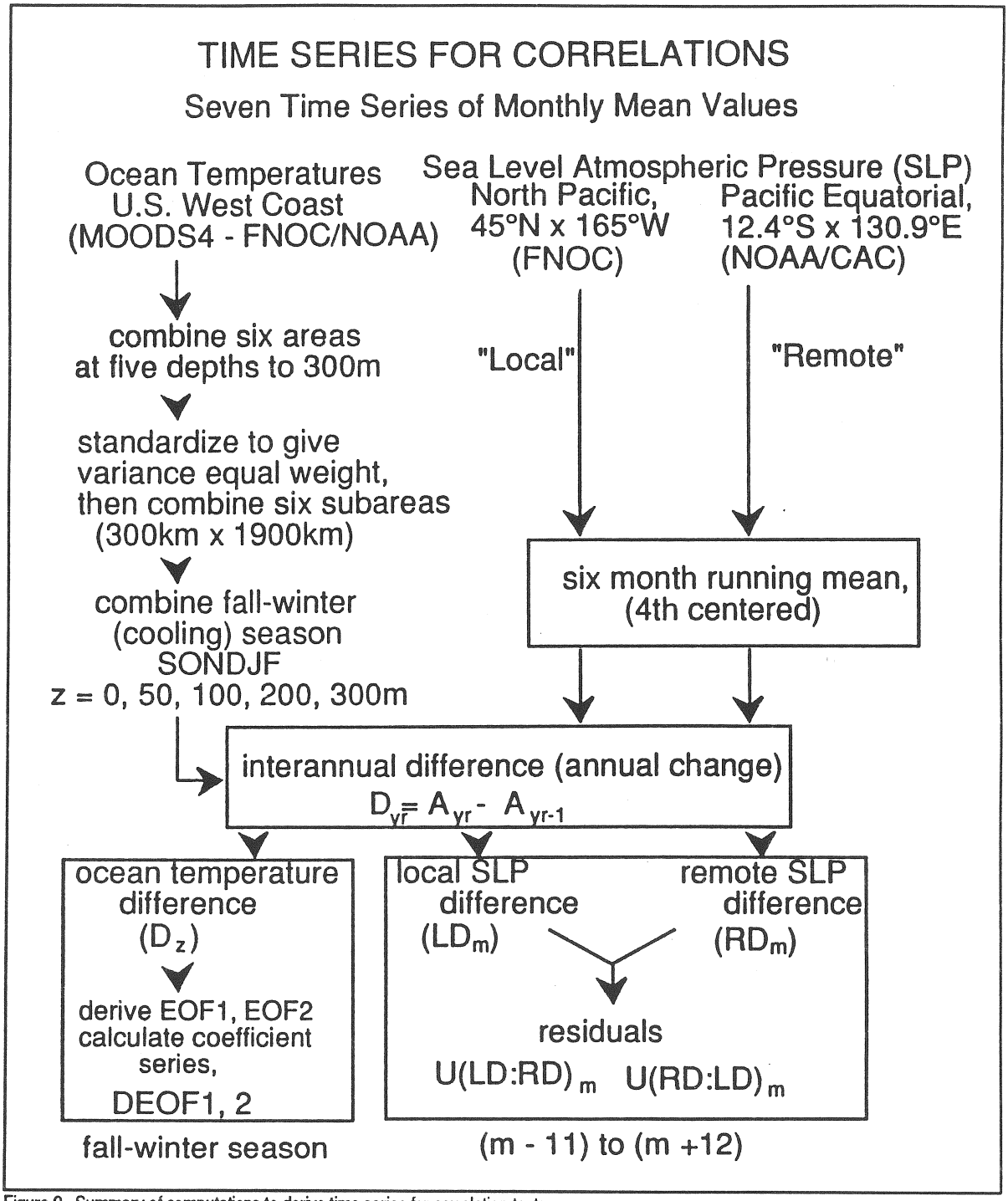

Figure 2. Summary of computations to derive time series for correlation tests.
All series used were either inter-annual differences of 7 monthly mean series (D_z, RD_m, LM_m) or derived from them (DEOF1, $U(LD:RD)_m$, *etc*).

cooling in the eastern equatorial Pacific. Monthly mean values for Darwin SLP were derived by averaging all daily values for the month. The series was then smoothed with a 6-month running mean, with the resulting mean values assigned to the fourth month. All "Pacific equatorial" or "remote" forcing indicators were derived from this smoothed series.

The monthly mean SLP at 45°N x 165° W in the northeastern Pacific was selected as an indicator of Aleutian Low cyclogenesis and large-scale local forcing. This location is not the center of greatest seasonal development of the Aleutian Low, but it is near the center of maximum seasonal variation (Horel and Wallace 1981). It is also one of the four locations used by Horel and Wallace (1981) to describe the Pacific-North American (PNA) teleconnection pattern. The monthly SLP at this location was derived by averaging the 6-hourly analyzed pressure fields produced at Fleet Numerical Oceanographic Center (63 x 63 northern hemisphere grid) for each month. The resulting series of monthly means was treated identically to the Darwin series. All "north Pacific" or "local" process indicators were derived from this smoothed series. Figure 2 summarizes the procedures used in deriving the series used in correlations.

Interannual changes or interannual difference indicators of ocean temperature, remote forcing, and local forcing are used in the correlation analyses. The interannual differences were computed for the current year (yr) by subtracting the parameter value for the previous year (yr-1), for example, for a particular annual value of ocean temperature change:

$$D_{z,yr} = A_{z,yr} - A_{z,yr-1}.$$

The five ocean temperature difference series are labeled "D_z" and the local and remote difference series are labeled "LD" and "RD," respectively (Figure 2).

If there are specific vertical patterns of ocean temperature change associated with remote and local forcing, they should be evident in Empirical Orthogonal Functions derived from the D_z matrix (Figure 3). The first two EOFs of D_z will be given physical interpretation drawn from correlations between the series of expansion coefficients (DEOF1 and DEOF2) and indicators of atmospheric forcing. The 50-meter series (D_{50}) was excluded from this part of the analysis to weight the EOFs equally with respect to depth interval, since distribution of anomaly over depth appears to be important in distinguishing between event type (Norton *et al* 1985a,b).

As noted, atmospheric teleconnections may link changes in SST in the equatorial Pacific to SLP over the north Pacific. This physical relationship causes the local and remote interannual difference indicators (LD, RD) to be correlated, especially in winter. To correct the LD and RD series for the atmospheric teleconnection, each was linearly regressed on the other, on a month-to-month basis, and the residual series used in correlation tests. The residual values represent the variability in the dependent variable unexplained by the independent variable. These series are referred to as "remote index residuals" or "U(RD:LD)" and "local index residuals" or "U(LD:RD)".

This approach may not show exact relationships between variables or remove all effects of the atmospheric teleconnection and its possible feedbacks but, like the other data manipulations described, it requires

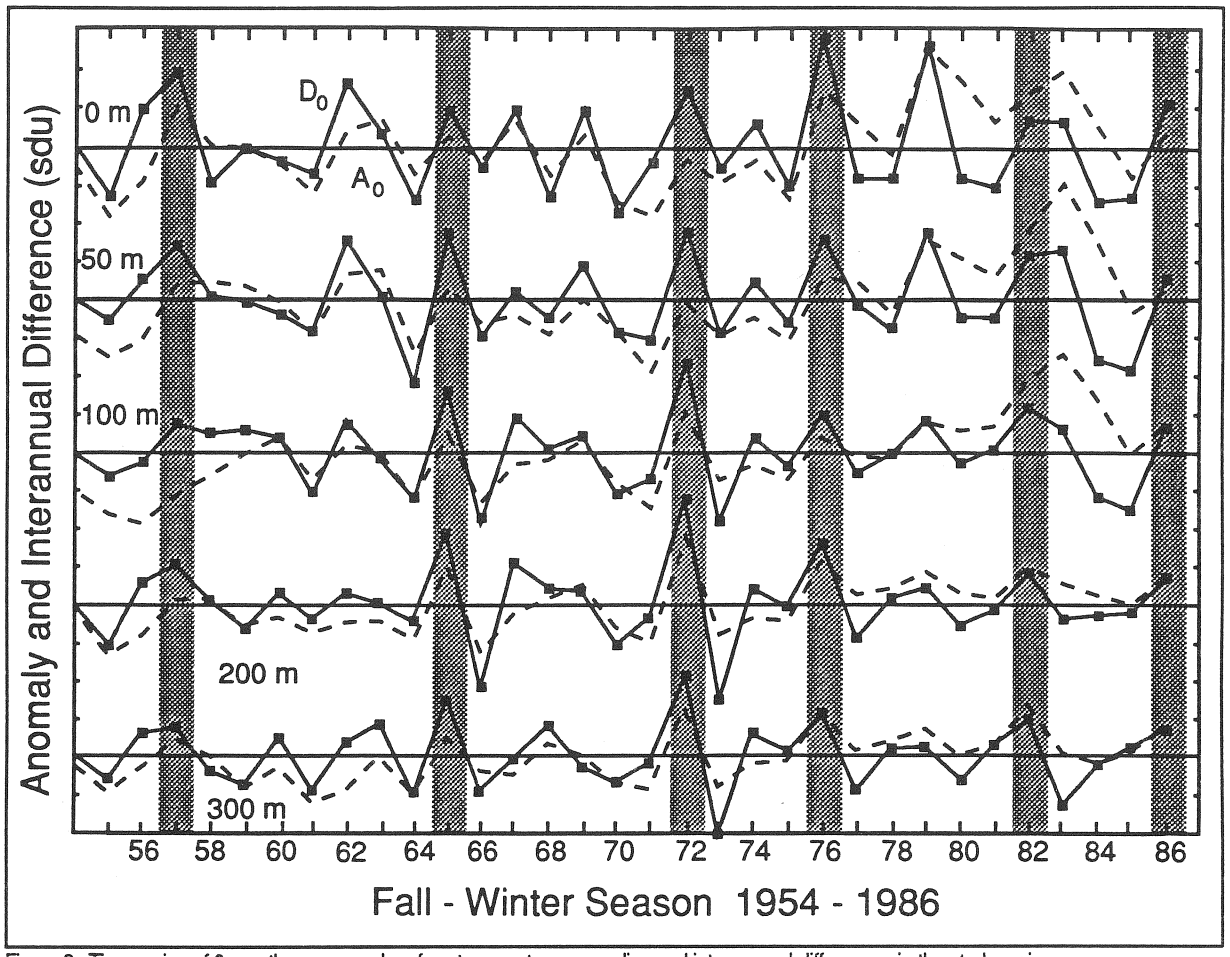

Figure 3. Time series of 6-month average subsurface temperature anomalies and inter-annual differences in the study region.
Solid lines indicate inter-annual temperature change for fall/winter combined (D_z).
Dotted lines indicate combined standardized temperature anomalies (A_z).
Horizontal lines mark zero anomaly and zero inter-annual change.
Zero value lines are two standard deviation units apart.
Shading indicates El Niño years.

minimal assumptions about the nature of the connecting processes. In the case of U(LD:RD), some correction is made for effects of the atmospheric teleconnection, but the interpretation of U(RD:LD) is less direct.

Results

In years when coherent ocean temperature changes extend from the surface to 300 meters depth, remote forcing from the equatorial Pacific is indicated (Figure 4). Correlation coefficients (r) between time series of year-to-year ocean temperature change along the West Coast and the indicator of Pacific equatorial atmospheric conditions (RD) were as large at 100 meters and below ($r > 0.7$, $p < 0.01$) as at the surface (Figure 4a). Figure 3 shows that during 1954 to 1986, the warming events that were coherent over the upper 300 meters occurred only during moderate to strong El Niño years (Quinn *et al* 1987). For fall/winter warming events that appear more closely related to local, north Pacific forcing, correlation coefficients were greater in magnitude at the surface ($r < 0.7$) than at 100 meters and below (Figure 4b). At the ocean surface, lags of up to 6 months

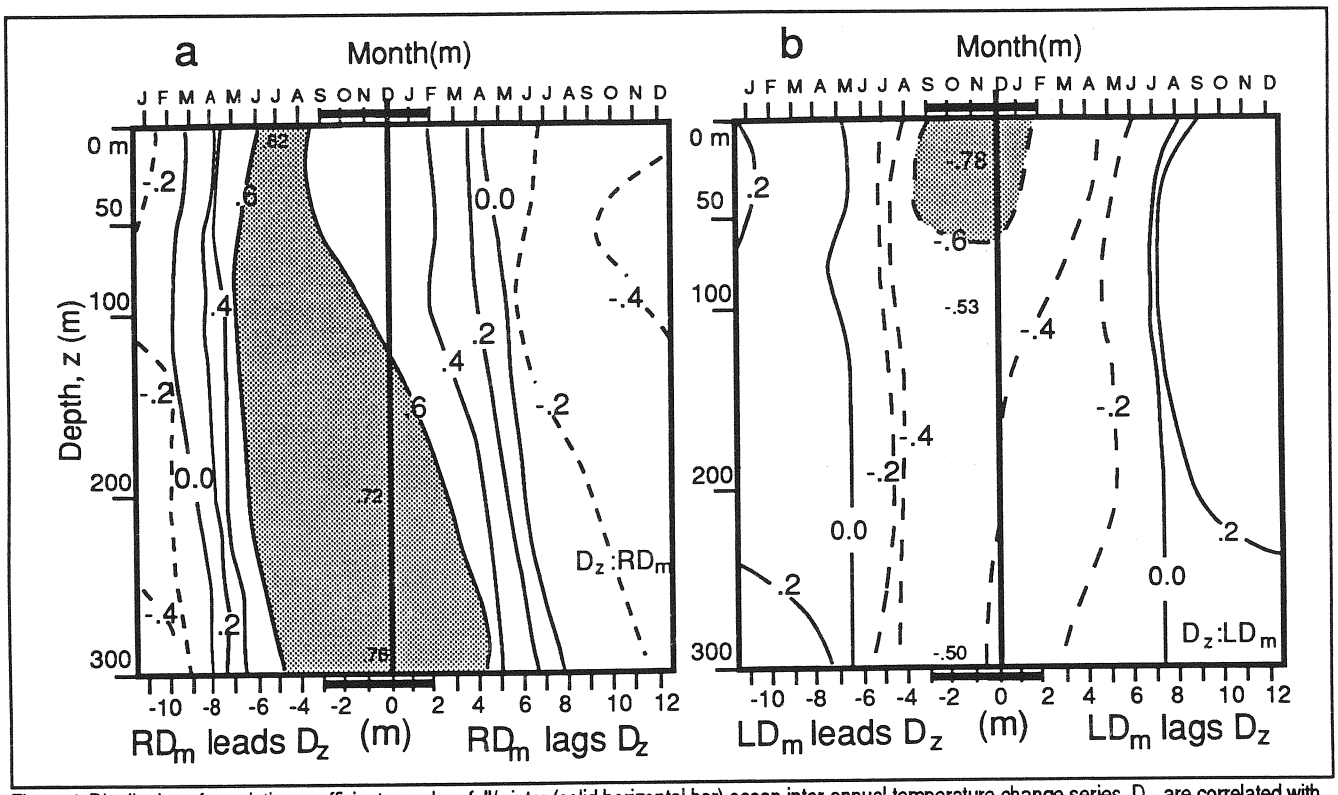

Figure 4. Distribution of correlation coefficients, r, when fall/winter (solid horizontal bar) ocean inter-annual temperature change series, D_z, are correlated with the remote (a) and local (b) inter-annual atmospheric pressure change series.
Variation in RD and LD is from January (m=11 leads in yr) through December (m+12 lags in year+1) of the following year.
The vertical line marks December of the event year (m=0 lags).
Solid and dashed contours at r=0.2 intervals show positive and negative correlation, respectively.
For |r| >0.4 and p <0.05. Areas where |r| is greater than or equal to 0.6 and p<0.01 are shaded.
Positive anomalies in the remote indicator (a) and negative anomalies in the local indicator (b) are correlated with anomalously high temperatures in the study region.

in maximum correlation were found for equatorial Pacific forcing (Figure 4a), while lags of 3 months or less were characteristic of local forcing (Figure 4b).

The first two EOFs accounted for more than 92.5 percent of the variance of the D_z time series (Figure 5). The first EOF accounts for 79.1 percent of the variance and has nearly uniform component loading over depth (upper panel, Figure 5a). In Figure 5a, a broken line traces the correlation of DEOF1 with the atmospheric forcing indices (LD, RD). From these correlations it appears that EOF1 is related to both the local and remote indices. However, when series residuals, U(LD:RD) and U(RD:LD), were correlated with DEOF1 (solid lines), only the correlation with the remote forcing index residual [U(RD:LD)] remained significant with $p < 0.05$ (greater than shaded area in Figure 5a, lower panel).

In Figure 5 the shaded areas represent the range of r values required for $p < 0.05$ when the range of effective degrees of freedom is between n and n*. Here n is the number of values in the correlated series and n* is the effective number of degrees of freedom as determined by the method of Chelton (1983).

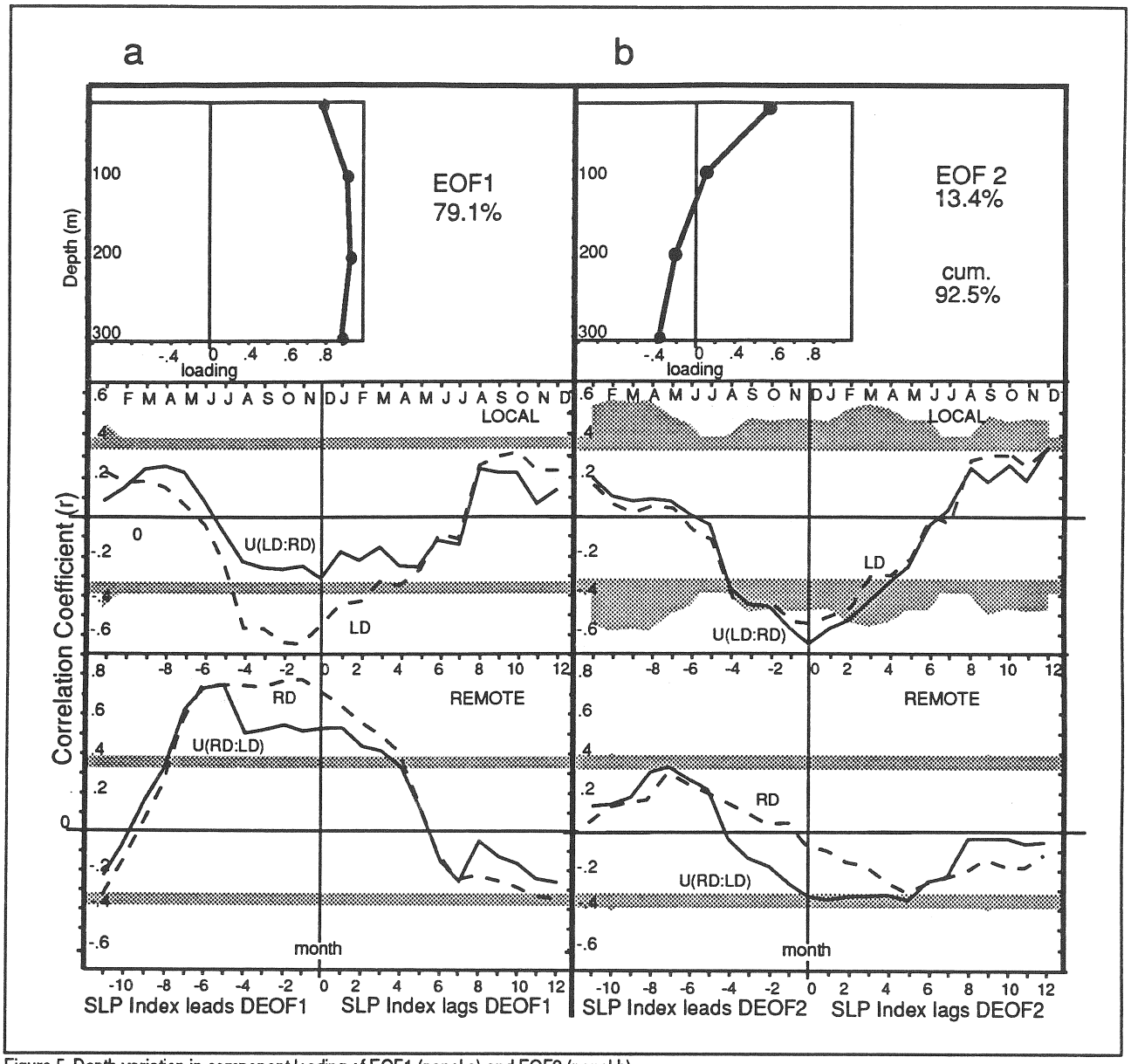

Figure 5. Depth variation in component loading of EOF1 (panel a) and EOF2 (panel b)

Variation derived from D_z is shown in the upper panels.

Percentage of variance explained by each EOF is on the upper right of each panel.

Broken lines in the middle and lower panels show the correlation of the time variation of coefficients of EOFs 1 and 2 (DEOF1 and DEOF2) to the atmospheric forcing indices LD_m and RD_m.

Correlation with the residuals $U(LD:RD)_m$ and $U(RD:LD)_m$ are shown by the solid lines.

Monthly leads and lags are the same as for Figure 4.

If r values exceed the upper bounds of the shaded area, $p < 0.05$ is indicated.

The second EOF accounts for 13.4 percent of the variance in D_z and reverses sign at depths below 100 meters (Figure 5b). This suggests that warming at 0 and 100 meters might be accompanied by cooling at 200 and 300 meters. The local, north Pacific, atmosphere appears to be important in forcing this variational mode, as shown by significant correlation in December in the middle panel of Figure 5b. The correlation coefficients for October (yr) through February (yr+1) clearly exceed the p=0.05 level (shaded) for correlations with both local forcing indices [LD, U(LD:RD)].

Discussion

The results show that northern coastal California Current warming episodes associated with Pacific equatorial events are detected by interannual temperature change at 100 meters and below, and warming associated with north Pacific influences are more likely to be detected in the surface layers, rather than at depth. The pattern of the deep signal is qualitatively consistent with effects expected from remote forcing through the ocean. Complex modal structures associated with coastal-trapped waves contribute to a signal that may be more pronounced at depth due to vertical propagation accompanying horizontal propagation (McCreary 1984; Romea and Allen 1983).

A summary of the temporal relationships of Pacific Basin events and processes associated with a typical El Niño warming are compared with results of the present study in Figure 6. In the upper panel, heavy dashed lines represent temporal relationships established by Horel and Wallace (1981), Cane (1983), Rasmusson and Wallace (1983), and Trenberth (1989). A physical interpretation of the interannual difference is that it represents change in the system over the differencing interval, or the processes that change the variable value during the differencing interval. These interpretations are illustrated by comparing the upper and lower panels of Figure 6.

The lower panel shows that the interannual change of remote forcing (RD) most highly correlated with ocean temperature change (D_Z) corresponds to the period of increasing SLP at Darwin during El Niño generation (top broken line). This correspondence implies that the interannual difference represents the accumulated effects of processes occurring over the differencing interval, *ie*, accumulated increase in sea level atmospheric pressure. This is qualitatively consistent with modeling results based on long wave theory (McCreary 1976, 1984; Shriver *et al* 1991).

Regional ocean temperature change and local forcing (LD) appear in phase, as shown by the upper and lower solid lines in Figure 6. However, phase shifts of less than 6 months might not be fully detected (resolved) in the present data treatment because of the high autocorrelation between consecutive values.

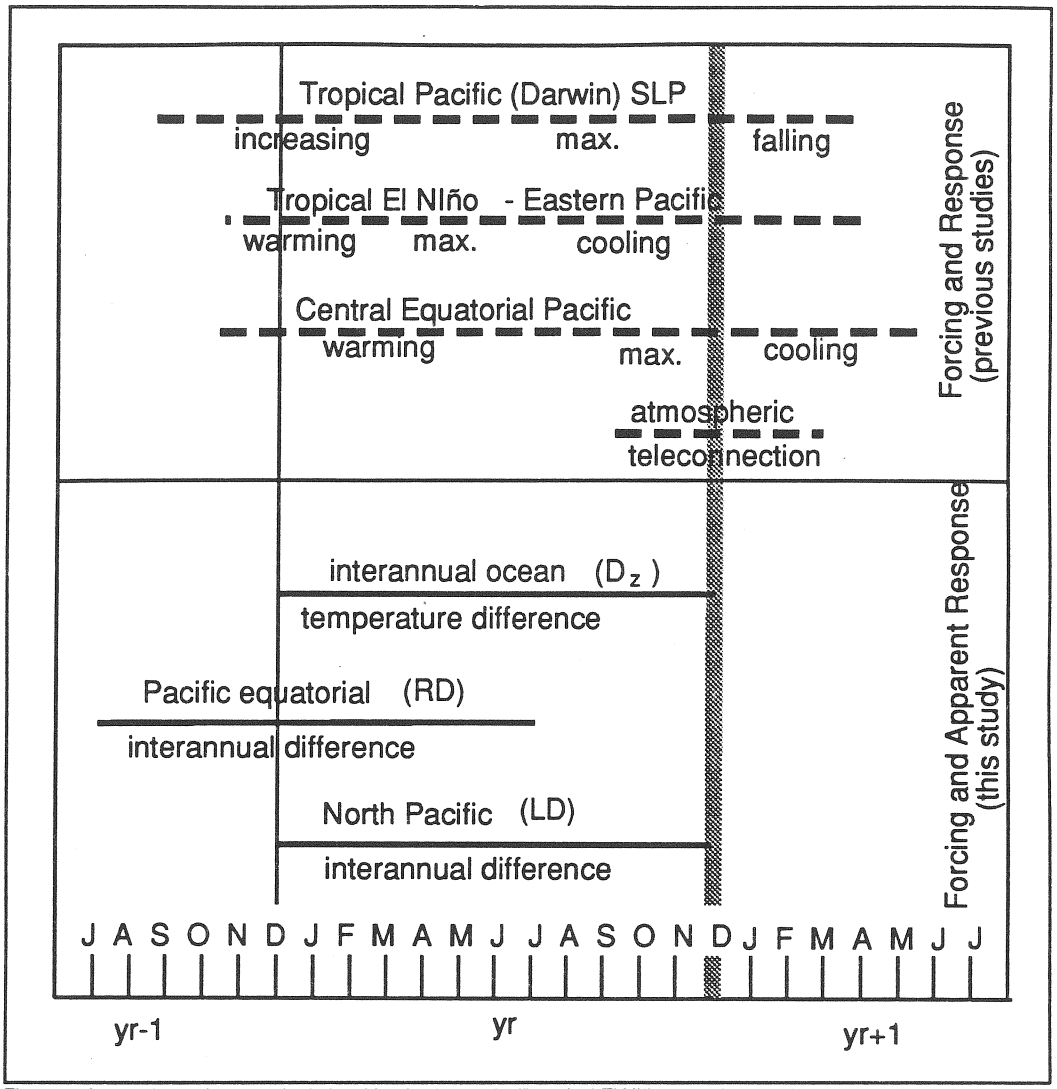

Figure 6. Comparison of temporal relationships for the "typical" tropical El Niño event (top) and results of this study (bottom).
Intervals of increase, maximum and decrease in SLP at Darwin, temperature change in the eastern and central equatorial Pacific, and corresponding Aleutian Low augmentation are shown by bold broken lines in the upper panel.
Solid lines summarize present results from Figures 4 and 5.
The upper solid line shows the ocean temperature differencing interval ; the vertical shaded line shows its temporal designation.
The lower two solid lines show the difference intervals of remote (SLP at Darwin) and local (North Pacific SLP) indicators that are most highly correlated with D_z.
Solid horizontal lines show the time intervals that will have greatest influence on the D_z, RD, and LD values.

Note

This paper is an abbreviated version of a manuscript by Norton and McLain that will be published elsewhere. A copy of the extended version is available from the authors.

References

Cane, MA. 1983. Oceanographic events during El Niño, *Science* 222:1189-1194.

Chelton, DB. 1983. Effects of sampling errors in statistical estimation, *Deep-Sea Res.* 30:1083-1103.

Clarke, AJ. 1983. The reflection of equatorial waves from oceanic boundaries, *J. Phys. Oceanogr.* *13*:1193-1207.

Emery, WJ, and K Hamilton. 1984. Atmospheric forcing of interannual variability in the northeast Pacific Ocean, *J. Geophys. Res.* 90:857-868.

Enfield, DB, and JS Allen. 1980. On the structure and dynamics of monthly mean sea level anomalies along the Pacific coast of North and South America, *J. Phys. Oceanogr.* 10:557-578.

Horel, JD, and JM Wallace. 1981. Planetary atmospheric phenomena associated with the Southern Oscillation, *Mon. Wea. Rev.* 109:813-829.

McCreary, JP. 1976. Eastern tropical response to changing wind systems: with application to El Niño, *J. Phys. Oceanogr.* 6:632-645.

_____. 1984. Equatorial Beams, *J. Mar. Res.* 42:395-430.

McLain, DR, RE Brainard, and JG Norton. 1985. Anomalous warm events in eastern boundary current systems, *Calif. Coop. Oceanic Fish. Invest. Rep.* 26:51-64.

Norton, JG, DR McLain, RE Brainard, and DM Husby. 1985a. El Niño event off Baja and Alta California and its ocean climate context. In Niño effects in the eastern subarctic Pacific Ocean, WS Wooster and DL Fluharty eds., pp. 44-72, Washington Sea Grant Program, University of Washington, Seattle.

Norton, JG, DR McLain, DM Husby, and RE Brainard. 1985b. Kelvin wave activity during recent California El Niños, *Eos Trans. AGU* 66:1295.

Quinn, WH, VT Neal, and SE Antunez de Mayolo. 1987. El Niño occurrences over the past four centuries, *J. Geophys. Res.* 92:14449-14461.

Rasmusson, EM, and JM Wallace. 1983. Meteorological aspects of the El Niño/Southern Oscillation, *Science* 122:1195-1202.

Romea, RD, and JS Allen. 1983. On vertically propagating coastal Kelvin waves at low latitudes, *J. Phys. Oceanogr.* 13:1241-1254.

Shriver, JF, MA Johnson, and JJ O'Brien. 1991. Analysis of remotely forced oceanic Rossby waves off California, *J. Geophys. Res.* 96:749-757.

Simpson, JJ. 1983. Large-scale thermal anomalies in the California current during the 1982-1983 El Niño, *Geophys. Res. Lett.* 10:937-940.

Trenberth, KE. 1989. TOGA and atmospheric processes, In Understanding climate change, A Berger, RE Dickinson, and John W Kidson eds., American Geophysical Union Geophysical Monograph 52, pp. 117-125, American Geophysical Union, Washington, DC.

Wallace, J, and D Gutzler. 1981. Teleconnections in the geopotential height field during the northern hemisphere winter, *Mon. Wea. Rev.* 109:784-812.